Bioactive Materials 27 (2023) 394–408

Contents lists available at ScienceDirect

Bioactive Materials

journal homepage: www.keaipublishing.com/en/journals/bioactive-materials

Review article

# Adipose-derived stem cell/FGF19-loaded microfluidic hydrogel microspheres for synergistic restoration of critical ischemic limb☆

Ruihan Wang [a,b,c,1], Fangqian Wang [d,e,1], Shan Lu [a,b,c,1], Bin Gao [a,b,c], Yuanqing Kan [a,b,c], Tong Yuan [a,b,c], Yisheng Xu [f], Chen Yuan [f], Daqiao Guo [a,b,c], Weiguo Fu [a,b,c,***], Xiaohua Yu [d,e,**], Yi Si [a,b,c,*]

[a] Department of Vascular Surgery, Zhongshan Hospital Fudan University, Shanghai, 200032, PR China
[b] Institute of Vascular Surgery, Fudan University, Shanghai, 200032, PR China
[c] National Clinical Research Center for Interventional Medicine, Shanghai, 200032, PR China
[d] Department of Orthopedics, The Second Affiliated Hospital of Zhejiang University School of Medicine, Hangzhou, 310009, Zhejiang, PR China
[e] Key Laboratory of Motor System Disease Research and Precision Therapy of Zhejiang Province, Hangzhou, 310000, Zhejiang, PR China
[f] State Key Laboratory of Chemical Engineering, East China University of Science and Technology, Shanghai, 200237, China

ARTICLE INFO

*Keywords:*
Microfluidic technology
Stem cell
Cytokine
Porous microspheres
Ischemic limb salvage

ABSTRACT

The efficacy of stem cell therapy is substantially compromised due to low cell survival rate and poor local retention post-delivery. These issues drastically limit the application of stem cells for ischemic limb therapy, which requires effective blood perfusion and skeletal muscle regeneration. Herein, based on microfluidic technology, an integrated stem cell and cytokine co-delivery system designed for functional ischemic limb salvage was constructed by first incorporating the myogenic cytokine, fibroblast growth factor 19 (FGF19), into microspheres composed of methacrylate gelatin (GelMA). Then adipose-derived stem cells (ADSCs) were highly absorbed into the porous structure of the microspheres, overcoming the insufficient loading efficiency and activities by conventional encapsulation strategy. The fabricated ADSCs/FGF19@μsphere system demonstrated a uniform size of about 180 μm and a highly porous structure with pore sizes between 20 and 40 μm. The resultant system allowed high doses of ADSCs to be precisely engrafted in the lesion and to survive, and achieved sustained FGF19 release in the ischemic region to facilitate myoblast recruitment and differentiation and myofibrils growth. Furthermore, the combination of ADSCs and FGF19 exhibited a positive synergistic effect which substantially improved the therapeutic benefit of angiogenesis and myogenesis, both *in vitro* and *in vivo*. In summary, a stem cell and cytokine co-delivery system with the properties of easy preparation and minimal invasiveness was designed to ensure highly efficient cell delivery, sustained cytokine release, and ultimately realizes effective treatment of ischemic limb regeneration.

## 1. Introduction

Arteriosclerosis obliterans (ASO), which affects more than 200 million people globally, is an ischemic disease caused by atherosclerotic stenosis in the lower extremities, and can progress to tissue loss, ulceration, or even gangrene in the lower limbs [1–3]. Despite its prevalence, the restoration of ischemic limb damage remains a significant challenge. As ASO progresses, the lack of blood perfusion causes local tissue necrosis; in turn, necrotic tissue generates oxidative stress and an inflammatory response, which inhibits the establishment of neovasculature [4,5]. Current clinical approaches such as endovascular stent implantation, balloon dilation, and vascular bypass can only restore blood patency to a

☆ Yi Si will handle correspondence at all stages of refereeing and publication, also post-publication.Peer review under responsibility of KeAi Communications Co., Ltd.

* Corresponding author. Fenglin Road 180, Shanghai, 200032, China.
** Corresponding author. Jiefang Road 88, Hangzhou, Zhejiang Province, China.
*** Corresponding author. Fenglin Road 180, Shanghai, China.
*E-mail addresses:* fu.weiguo@zs-hospital.sh.cn (W. Fu), xiaohua.yu@zju.edu.cn (X. Yu), si.yi@zs-hospital.sh.cn (Y. Si).

[1] These authors share first authorship of this article.

https://doi.org/10.1016/j.bioactmat.2023.04.006
Received 8 October 2022; Received in revised form 19 March 2023; Accepted 4 April 2023

certain extent instead of impeding ASO progression. Moreover, these conventional therapies are mostly focused on blood flow reconstruction, and they fail to directly regenerate damaged skeletal muscle, leading to extensive fibrosis formation and permanent impairment of myofibrils [6–8]. Therefore, novel strategies capable of supporting blood perfusion reconstruction as well as restoring skeletal muscle functions are urgently needed in the context of salvaging ischemic limb damage.

Currently, a variety of therapeutic approaches such as stem cells, growth factors, gene vectors and other angiogenic inducers have been proposed to rescue ASO-induced limb damage [9–12]. These approaches can induce angiogenesis by directly promoting neovascularization or encouraging the recruitment of host angiogenic cells. Among these approaches, stem cell therapy stands out as an emerging strategy due to its self-renewal ability, paracrine secretion, and multilineage differential potential [13,14]. For example, adipose-derived stem cells (ADSCs) could not only directly differentiate into vascular endothelial cells to realize neovascularization, but also secrete miRNA-containing or cytokine-containing vesicles in a paracrine manner to regulate the proliferation, differentiation and immunomodulation of neighboring cells [15–21]. For instance, Madonna et al. directly injected ADSCs suspension into the ischemic lesions and established neovascularization, as ADSC can mediate the hypoxia-induced release of cytokines (VEGF and related growth factors) and give rise to angiogenesis [22]. However, several challenges remain to be addressed before its clinical translation: i) mechanical damage to cells by injection due to fluid shear stress [23]; ii) cell loss and leakage to surrounding tissues [24]; and iii) low survival rate due to redox imbalance, immune response, and lack of cell-cell and cell-matrix interactions [25]. It has been reported that less than 3% of the injected cells survived and reached the therapeutic sites after their administration [26]. Such a small number of cells reaching the lesion would limit the regenerative performance and render therapeutic benefits irreproducible [27,28]. Hence, there is considerable demand for an injectable stem cell delivery system capable of enhancing the delivery efficacy of stem cells to maximize their therapeutic potency. The ideal cell delivery systems should not only allow cells to be transplanted precisely and efficiently to the targeted site, but also provide cells with a conducive microenvironment to improve cell engraftment, survival, and retention.

ASO also leads to significant skeletal muscle loss due to atrophy or necrosis after ischemia, which is difficult to restore on its own [6]. Even the neovascularization is mostly completed, the regeneration of skeletal muscle yet fails to recover. Nonetheless, a recent study showed that the pharmaceutical treatment of fibroblast growth factor 19 (FGF19) is a novel strategy to solve muscle-atrophy-related conditions [29]. Skeletal muscle is a direct target of FGF19 through expression of the β-Klotho receptor. *In vivo*, FGF19 has been shown to potently promote myoblast differentiation and muscle cell growth by phosphorylating S6K1 and ERK1/2. Mice treated with FGF19 have displayed higher skeletal muscle mass and better muscle strength [29,30]. These results suggest that FGF19 possesses appealing advantages in restoring skeletal muscles after ischemia. However, the systematic administration of FGF19 is a suboptimal approach for ischemic limb recovery for several reasons, including: i) its relative short-term efficacy; ii) the inability to localize it to the ischemic lesion; and iii) its high cost due to the large dosages needed. Therefore, a long-acting drug delivery system, whereby FGF19 could be released sustainedly and precisely at the location of ischemic lesions, is preferred. Additionally, the literature also supports that FGF19 may realize a synergistic effect with stem cell therapy to comprehensively improve the therapeutic effects of ASO-induced lower extremity ischemia [31].

Based on the aforementioned considerations, we aimed to design a growth factor-incorporated stem cell delivery construct via our highly efficient, microsphere-assisted system. Gelatin methacrylamide (GelMA) is a photopolymerized hydrogel that demonstrates controllable biodegradability, excellent biocompatibility, and tunable mechanical strength. It has been extensively used in the application of tissue restoration due to its tunable physiochemical capacity. After photocrosslinking, it exhibits stable mechanical property that favors cell adhesion, proliferation, and planting, which is considered to be an ideal biomaterial for cell transplanting and cytokine delivery. Leveraging on inherent bioactivity of GelMA, in this study, we proposed a novel ischemic limb restoration strategy by combining the efficient delivery of localized high-density ADSCs together with the *in situ* sustained release of FGF19 to promote neovascularization, and skeletal muscle restoration simultaneously, thereby demonstrating a potential innovative and promising clinical application of the strategy in the lower extremity ischemia. Specifically, FGF19 was incorporated into GelMA microspheres leveraging our one-step innovative microfluidic technology to fabricate FGF19-loaded GelMA microspheres. The ADSCs were then spontaneously absorbed into the porous structure formed during lyophilization on the microspheres, in order to construct the ADSC/FGF19@μsphere system. The resultant ADSC/FGF19@μsphere system was amenable to a minimally invasive injection into the ischemic lesion site and exhibited outstanding angiogenic and myogenic properties (Fig. 1). We demonstrated that our microfluidic device could generate homogenous micro-droplets of GelMA to fabricate microspheres with properties of narrow particle size distribution and high reproducibility. In addition, GelMA microspheres allowed high FGF19 loading efficiency as well as the sustained release of FGF19 *in situ*, which could generate myogenesis in a long-acting manner. Further, the freeze-drying GelMA microspheres with a highly porous structure could serve as a perfect stem cell carrier, maintaining a microenvironment that favors ADSCs survival, proliferation, and differentiation. More importantly, this system showed considerable enhancement of myogenesis and angiogenesis, suggesting that co-delivery of ADSCs and FGF19 broke the vicious cycle of ischemia-muscle atrophy, allowing to exert a synergistic therapeutic effect for ischemic limbs. Collectively, our data indicate that ADSC/FGF19@μsphere system could be a promising strategy to achieve synergistic effect on functional ischemic limb salvage.

## 2. Methods

### 2.1. Synthesis of GelMA

GelMA was synthesized as described previously [32]. Briefly, the 10% (w/v) gelatin was dissolved into Dulbecco's phosphate-buffered saline (DPBS) (Invitrogen, San Diego, CA) at 60 °C. The methacrylic anhydride (MA) (0.8 mL per *g* gelatin) was supplemented to react with gelatin for 3 h under vigorous stirring at 50 °C. Then, the solution was added into a 5-fold dilution with warm (40 °C) DPBS to stop the reaction. The resultant solution was dialyzed in distilled water at 40 °C for 1 week. Afterwards, the purified solution was freeze-dried for 7 days, forming a white porous foam, which could be stored at −80 °C for further use.

### 2.2. Microfluidic production of FGF19-loaded microspheres

(I) $^{1}$H magnetic resonance spectroscopy (NMR): The degree of methacrylation was calculated as the ratio of the number of reacted methacrylamide groups to the number of amine groups. 30 mg GelMA was fully dissolved in deuteroxide. Using magnetic resonance spectroscopy (NMR) (Varian Inova 500), these values were obtained by integrating peaks at 5.4 and 5.7 ppm, which corresponded to methacrylamide groups. (II) Fabrication of FGF19-loaded microspheres: In order to prepare the FGF19 solution, 50 μg FGF19 was supplemented into the 5 wt% GelMA solution containing 0.5 wt% photo-initiator, which served as the dispersed phase. Isopropyl myristate oil served as the continuous phase. These two phases were injected into different microchannels and the dispersed phase formed monodisperse droplets. The flow rates of the water phase and the oil phase were adjusted to obtain droplets of sizes <200 μm. The collected microdroplets were photopolymerized into microspheres upon exposure to UV irradiation

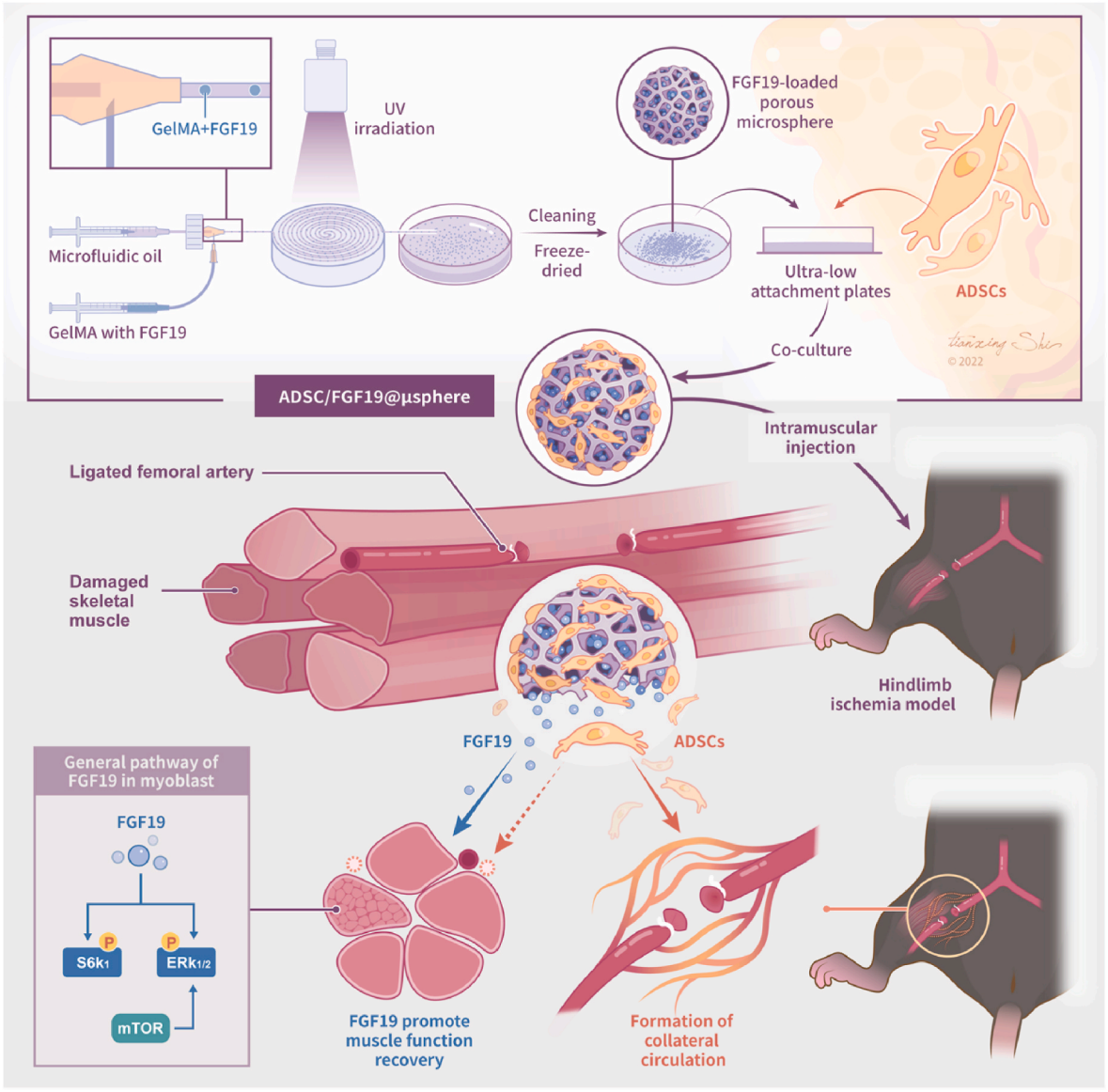


**Fig. 1. Schematic illustration of the synthetic process of ADSC/FGF19@μspheres and ischemic limb restoration.** Uniform droplets of GelMA hydrogel with FGF19 were first prepared with the assistant of microfluidic technology, followed by rapid light crosslinking and freeze-drying to obtain FGF19-loaded porous microspheres. ADSCs were then loaded into the microspheres by absorption to construct the ADSC/FGF19@μsphere. The resultant ADSC/FGF19@μsphere was injected into the ischemic hindlimb, wherein it realized highly efficient ADSCs delivery and sustained release of FGF19 to facilitate the simultaneous neovascularization and skeletal muscle restoration.

(365 nm, 3 min). The FGF19-loaded microspheres were thoroughly extracted in cleansing water, and then purified in PBS. We used microscope images and Image J software to determine the size of the resultant FGF19-loaded microspheres.

### 2.3. Physical characterization of FGF19-loaded GelMA microspheres

(I) Surface morphology: To exam the surface morphology of the microspheres, scanning electron microscopy (SEM) (S-4800; Hitachi, Kyoto, Japan) was used. (II) FGF19 release: The *in vitro* release profile of FGF19 from GelMA microspheres was investigated for a 7-day period. 500 μL microspheres were placed in tubes containing 500 μL PBS at 37 °C. At predetermined time points, the storage solution was removed for fluorescence test and replaced with 500 μL PBS. The concentration of FGF19 released from microspheres was determined using an FGF19 ELISA Kit (R&D systems, Minnesota, USA) according to the manufacturer's protocol. Briefly, 50 μL of the obtained storage solution was added into a 96-well FGF19 microplate that previously coated with monoclonal antibody. After three washes with the buffer in the kit, 200 μL of FGF19 conjugate was added into each sample followed by 2 h incubation. The samples were washed again and 200 μL of FGF19 substrate was added into each well before incubating in the dark at room temperature for 30 min 50 μL of stop solution was then added into each well and the optical density was determined using a microplate reader at 485 nm wavelength. The amount of cytokine released at different time points and the cumulative percentage of released FGF19 relative to the total amount in each sample were then converted. (III) Swell capability: The 10 mg freeze-drying microspheres were placed in a 1.5 mL EP tube, dispersed in 1 mL PBS and left undisturbed for 3 h. To observe the swelling, 500 μL of the microsphere solution was observed under a light microscope. After wiping off the moisture of the microspheres, the weights of microspheres were measured and calculated. (IV) Degradation: To mimic the physiology environment, 10 mg freeze-drying microspheres were incubated at 37 °C with 500 μL of PBS containing 2 U

mL −1 of collagenase type II in 1.5-mL tubes for 7 days. Collagenase-containing PBS was replaced every day to ensure constant enzymatic activity. At the pre-determined time points, the PBS was removed from tubes and the samples were washed twice with sterile deionized water. Then, the deionized water was removed and the microspheres were freeze-dried for 24 h for residual weight measurement. The following equation was used to calculate percentage degradation: $D\% = \frac{W_0 - W_t}{W_0} \times 100\%$. (V) Stiffness: The stiffness measurements on microspheres were performed by the atomic force microscopy (AFM) assay. AFM assay: Force measurements on the microspheres were performed using AFM-assisted nanoindentation as previously described [32]. The AFM (Bruker Dimension® FastScan™) was used for measurements. A tipless silicon nitride cantilever (NSG-10) was located and positioned over the center of the microspheres. The probe velocity was 200 nm/s. The morphology of the microspheres was measured in PeakForce Tapping mode, and the force-displacement curves were recorded. All tests were performed at 25 °C and 40% relative humidity.

### 2.4. Biocompatibility of the microspheres

(I) Cell culture: Murine adipose-derived stem cells (ADSCs) and mouse myoblasts (C2C12) were purchased from Cyagen Biotechnology Co., Ltd (Suzhou, China). The cells were cultured in Dulbecco's modified Eagle medium (DMEM) supplemented with 10% fetal bovine serum (FBS) at 37 °C in a humidified incubator containing 5% $CO_2$. The medium was replaced every 2 days, and the cells of passages 3 to 4 were harvested for subsequent experiments. (II) Loading of ADSCs into microspheres: Before loading the cells, the microsphere scaffolds were immersed in 75% alcohol until the alcohol was completely volatilized and irradiated under UV light for 12 h for sterilization. Then, 200 μL of ADSCs suspension ($5 \times 10^6$/mL) was mixed with 10 mg of microspheres and the mixture was transferred to ultra-low attachment plates (Corning, NY, USA). The ADSCs and the microsphere scaffold were co-incubated at 37 °C for 8 h to allow cell attachment to the microsphere scaffold. (III) Cell adhesion: To observe cell adhesion on microspheres, staining of F-actin and cell nuclei was performed using phalloidin (Beyotime, Shanghai, Chin) and DAPI (Sigma), respectively. Staining was conducted according to the manufacturer's instructions. Briefly, after washing by PBS, the samples were fixed by 4% paraformaldehyde for 40 min, permeabilized by 0.1% Triton X-100 for 30 min, and blocked by 1% BSA for 40 min. Samples were incubated in phalloidin solution for 40 min, and then in DAPI solution for 5 min at 37 °C. The positively labelled cells were detected using a fluorescence microscope. (IV) Cell survival and proliferation: After the ADSCs had co-incubated with the microsphere scaffold for the stipulated time, the microspheres were stained with the Calcein-AM/Propidium iodide. (V) Live/Dead cell Double Staining Kit (Abnova Diagnostics, Dongguan, China), following the protocols provided by the manufacturer to determine the ADSCs survival on the microsphere scaffold. The morphology and cell distribution of the microspheres were observed under a fluorescence microscope. Considering further cell proliferation on the microsphere scaffold, the ADSCs viability was detected by the Cell Counting Kit-8 (CCK-8) assay (Beyotime, Shanghai, China). To show that the microsphere did not limit the proliferation of ADSCs, ADSCs or ADSCs-laden microspheres were cultured in new plates for 1, 2, 3, 5, and 7, separately. After incubation with CCK-8 Detection Kit for 2 h, drawing 100 μL of culture medium (containing 10% CCK-8 solution) from each group to a new 96-well plate. The absorbances were detected at a wavelength of 450 nm with a microplate reader.

### 2.5. Angiogenic and migration activity of ADSCs on microspheres

Six groups of ADSCs with different densities (low density: $1 \times 10^5$ cells, medium density: $5 \times 10^5$ cells, and high density: $1 \times 10^6$ cells) were attached to 10 mg blank microspheres and FGF19-loading microspheres, respectively. The following steps were implemented. (I) Quantitative real-time PCR (qRT-PCR): After the cell attachment, total RNA was extracted from all of the samples using Total RNA Isolation Reagent (Trizol; Invitrogen Life Technologies Inc., Carlsbad, CA, USA) according to the manufacturer's protocol. Using HiScript Reverse Transcriptase (Vazyme Biotech Co. Ltd., Nanjing, China) to synthesize cDNAs. RT-PCR was performed on an ABI7900 RT-PCR system (Applied Biosystems; Foster City, CA, USA) by using SYBR Green (Vazyme Biotech Co. Ltd., Nanjing, China) following the instructions provided by the manufacturer. Relative mRNA expressions were normalized against β-actin, and relative gene expressions were determined using $2^{-\Delta\Delta Ct}$. (II) Western blot analysis: Cells were harvested in RIPA lysis buffer (Beyotime, Haimen, China) following the manufacturer's protocol. A BCA Protein Assay kit (ThermoFisher Scientific, Waltham, MA, USA) was used to quantify the protein content. Proteins were separated on 10% SDS-PAGE gel, and transferred to PVDF membranes (Millipore Corp., Burlington, MA, USA). The membranes were incubated with antibodies to collagen I (1:1000; Servise), collagen IV (1:1000; Abcam), laminin (1:1000; Abcam), fibronection (1:1000; Abcam), HGF (1:1000; Affinity), VEGF (1:1000; Abcam), bFGF (1:1000; Affinity) and β-actin (1:2000; Abcam). Signals were detected using an enhanced chemiluminescent reagent (Pierce, Rockford, IL, USA). (III) Scratch wound healing assay: Control ($1 \times 10^6$ ADCSs only) and $1 \times 10^6$ ADSCs attached to the microsphere scaffold were seeded in 6-well plates (Costar, 3596), respectively. After incubation with DMEM until the ADSCs on the microsphere adhered to the plate, the residual microspheres were washed off by DMEM, a sterile pipette tip was used to inflict a 0.8 mm linear scratch wound in the center of the cell monolayer. The wounds were monitored under the phase contrast microscope, and measurements of the scratch width were calculated using ImageJ v. 1.50 (National Institutes of Health, Bethesda, MD, USA). (IV) Transwell assay: To investigate whether the migration efficiency of ADSCs was affected by the microspheres, an 8 μm transwell plate (Corning, 3422) was used. The ADSCs harvested from a conventional plate and microsphere were seeded in the upper chamber, and DMEM medium was added into the lower chamber, respectively. After 12 h of incubation at 37 °C, ADSCs were stained with 0.5% crystal violet solution, and the cell intensity was measured.

### 2.6. Effects of FGF19-loaded microspheres on myoblasts

(I) Cell culture: The mouse myoblast (C2C12 cell line) was purchased from Cyagen Biotechnology Co., Ltd (Suzhou, China). The cells were cultured in DMEM (High Glucose) (Gibco, Life Technologies, Grand Island, NY, USA) supplemented with 10% FBS (Gibco) and 1% P/S (Pall Corporation) at 37 °C in a humidified incubator containing 5% CO2. The medium was replaced every 2 days, and the cells of passages 3 to 4 were harvested for subsequent experiments. (II) qRT-PCR: To explore whether FGF19-loaded microspheres could promote the myogenic RNA content of myoblasts, 3 typical myogenic genes (Pax7, MyoD, and Myf5) in C2C12 cells co-cultured with FGF19-loaded microspheres for 3 or 5 days were detected. Total RNA was extracted from all of the samples using Trizol (Invitrogen Life Technologies Inc., USA), according to the manufacturer's protocol. Using HiScript Reverse Transcriptase (Vazyme Biotech Co. Ltd.) to synthesize cDNAs, qRT-PCR was performed on the ABI7900 RT-PCR system (Applied Biosystems, Foster City, CA, USA) using SYBR Green (Vazyme Biotech Co. Ltd.), following the instructions provided by manufacturer. Relative mRNA expressions were normalized against β-actin, and relative gene expressions were determined using $2^{-\Delta\Delta Ct}$. (III) Western blot analysis: For the above C2C12 cells, total proteins were collected. Cells were harvested in RIPA lysis buffer (Beyotime, Haimen, China) following the manufacturer's protocol. A BCA Protein Assay kit was used to quantify the protein content. Proteins were separated on 10% SDS-PAGE gel, and transferred to PVDF membranes (Millipore Corporation, MA, USA). The membranes were incubated with antibodies to Pax7 (1:1000; Abcam), MyoD (1:1000;

Affinity), Myf5 (1:1000; Abcam) and β-actin (1:2000; Abcam). Signals were detected using an enhanced chemiluminescent reagent (Pierce, Rockford, IL, USA). (IV) Transwell assay: To investigate whether FGF19-loaded microspheres could promote the migration function of myoblasts *in vitro*, an 8 μm transwell plate (Corning, 3422) was utilized. Briefly, $10^5$ C2C12 cells were seeded in the upper chamber. Then, FGF19-loaded microspheres and blank microspheres were added to the medium and maintained for 3 or 5 days. After that, the cells were collected, and the cell intensity was measured. (V) Phosphorylation of ERK1/2 and ribosomal protein S6 kinase (S6K1): To investigate the mechanism by which FGF19 promotes myoblast function, the primary rabbit anti-S6K1 (1:1000; Abcam), anti-phosphorylated S6K1 (p-S6K1) (1:1000; Cst), anti-ERK (1:1000; Affinity), anti-phosphorylated ERK (p-ERK) (1:1000; Affinity) and mouse anti-β-actin (1:2000; Abcam) were used in the test. Briefly, C2C12 cells were co-cultured with FGF19-loaded microspheres or blank microspheres for 3 days. Cells were harvested in RIPA lysis buffer (Beyotime, Haimen, China) following the manufacturer's protocol. A BCA protein assay kit was used to quantify the protein content. Proteins were separated on 10% SDS-PAGE gel, and transferred to PVDF membranes (Millipore Corporation, MA, USA). The membranes were incubated with antibodies to p-S6K1, S6K1, p-ERK and ERK at 4 °C overnight. Signals were detected using an enhanced chemiluminescent reagent (Pierce, Rockford, IL, USA).

### 2.7. Synergistic effect of FGF19 and ADSCs

To mimic the environment in which the fabricated ADSC/FGF19@μsphere system exerts its therapeutic effects of angiogenesis and myogenesis, we used the transwell assay to investigate the promoting effect of the ADSC/FGF19@μsphere system on myoblasts and the activities of ADSCs. (I) Transwell migration assay: To investigate whether the combined use of ADSCs and FGF19 had a stronger promoting effect on the myogenesis of C2C12 cells compared to the use of ADSCs or FGF19 alone, an 8 μm transwell plate (Corning, 3422) was utilized to mimic the microenvironment *in vivo*. Briefly, $10^5$ C2C12 cells were seeded in the upper chamber. The lower chamber contained the following: i) blank control, ii) blank microspheres, iii) FGF19@μspheres, iv) ADSC@μspheres, and v) ADSC/FGF19@μspheres. After 24 h to allow transmigration, the C2C12 cells were collected and stained with 0.5% crystal violet solution, and the cell intensity was measured. (II) Transwell co-culture assay: a 0.4 μm transwell plate was utilized to mimic the microenvironment *in vivo*, and i) blank control, ii) blank microspheres, iii) FGF19@μspheres, iv) ADSC@μspheres, and v) ADSC/FGF19@μspheres were added to the upper chambers, respectively, and $10^5$ C2C12 cells were seeded in the lower chambers and maintained for 2 days. Then, the C2C12 cells in the lower chamber and the ADSCs in the upper chambers were collected. (III) Western blot analysis: To analyze the myogenic activity of the C2C12 cells in the different groups, the proteins were collected. Briefly, C2C12 cells were harvested in RIPA lysis buffer (Beyotime, Haimen, China) according to the manufacturer's protocol. A BCA protein assay kit was used to quantify the protein content. And proteins were separated on 10% SDS-PAGE gel, and transferred to PVDF membranes (Millipore Corporation, MA, USA). The membranes were incubated with antibodies to MyoD (1:1000; Affinity) and β-actin (1:2000; Abcam). Signals were detected using an enhanced chemiluminescent reagent (Pierce, Rockford, IL, USA). (IV) Immunofluorescence staining: The ADSCs in groups iv) and v) were harvested and immunofluorescently stained with CD31 and MyhC, and examined under a fluorescence microscope.

### 2.8. In vivo ischemic limb restoration via ADSC/FGF19@μsphere

(I) Mice ischemic hindlimb model: The *in vivo* experiment was approved by the Animal Ethics Committee of Zhongshan Hospital Fudan University (Shanghai, China). The mice ischemic hindlimb model was performed as previously described [33]. Briefly, after the male C57BL/6 mice (8–10 weeks) mice were anesthetized by inhalation of sevoflurane, a 1 cm skin incision was made between the inguinal ligament and the knee joint to expose the femoral artery. The femoral artery was ligated with a 5-0 silk suture and excised. In the treatment scheme, the mice ischemic models were divided into 4 groups: (a) blank control (n = 10), (b) FGF19@μsphere (n = 12), (c) ADSC@μsphere (n = 12), and (d) ADSC/FGF19@μsphere (n = 12). The different treatment mixtures were suspended in PBS, and 100 μl suspensions (density of ADSCs: $5 \times 10^6$/mL) were rapidly injected into 3 different sites of the ischemic hindlimb using a 24-gauge needle. We used PBS in the blank control group. (II) Blood perfusion evaluation: Blood perfusion of the hindlimbs was performed on a Laser Doppler blood flow meter (MoorLDI2-HIR; Moor Instruments Ltd, Devon, UK). Briefly, with the mice in the supine position under anesthesia, the doppler blood flow signals were detected by 180 × 200 pixels from the lower abdomen to the knee joint. Then, 2 rectangle areas (20× 30 pixels) were drawn between the inguinal ligament and the knee joint of the ischemic limb and normal limb respectively, and were selected as the representative regions of interest (ROI) to calculate the perfusion values. The perfusion ratio between the ischemic side and the normal side was used as the indicator of the successfully induced model (perfusion ratio <0.2) and blood perfusion recovery. A Laser Doppler blood flow meter was used on post-operative days 0, 3, 7, 14, and 21 post-operation. (III) Histological evaluation: At 21 days after surgery, the hindlimb muscles from the ischemic zone were collected for histological analyses. After being fixed with paraformaldehyde solution and dehydrated, all of the muscles were embedded in paraffin and cut into 5 μm sections and the H&E and Masson's staining were then performed according to standard protocols to examine muscle degeneration and fibrosis formation. The pathological changes were observed under the microscope. (IV) Immunofluorescence staining for angiogenesis and myogenesis quantifications: Ischemic hindlimb muscles of all of mice in the groups were collected 21 days after the treatment. The tissue sections (10 μm) were immunofluorescently stained with VEGF (Abcam, USA) and MyoD (Abcam, USA) and examined using a fluorescence microscope. For quantitative analysis, 5 images were randomly selected from each slide and the immunofluorescence optical density was analyzed using ImageJ software. (V) Strength of grip: Muscle strength was recorded using a grip-test meter system (XR501, XinRuan, Shanghai, China). Mice were allowed to hold on to a metal grid with the ischemic paws and were gently pulled backwards until the animals could no longer hold the grid. Each mouse was given four trials, and average values were used to represent the muscle-grip strength of an individual mouse. Investigator was blinded to the animal-group treatment. (VI) Skeletal muscle contractility: The skeletal muscle contractility test was prepared as previously described [34–36]. Briefly, tibialis anterior muscles were collected from each group (n = 6), and were mounted vertically between two parallel wire electrodes. Then, the tendons were attached to the clips and connected to a force transducer (JZ101, Yilian Medicine, Shanghai, China). The muscles were kept moist using 37 °C Ringer's solution. Electricity (250 Hz, 25 V for 1 s) was used to evoke tetanic muscle contraction. The interval between each contraction was at least 5 min. The differences between the maximum contraction force and baseline were recorded, and then normalized to muscle mass. (VII) Tissue inflammation: In the tissue inflammation scheme, fifteen mice ischemic models were randomly divided into 5 groups. Three mice were injected with saline at the ischemic site as controls. The others were injected with blank microspheres, FGF19@μsphere, ADSC@μsphere, and ADSC/FGF19@μsphere. On day 3, the ischemic hindlimb skeletal muscles and plasma were collected. After being fixed with paraformaldehyde solution and dehydrated, all of the muscles were embedded in paraffin and cut into 5 μm sections and the H&E staining was then performed according to standard protocols to examine tissue inflammation. The levels of inflammatory factors (TNF-α, IL-6, and IL-1β) in the plasma were detected by ELISA Kits followed by the manufacturer's protocol.

### 2.9. Statistical analysis

All quantitative results were obtained from at least triplicate samples. Data were expressed as mean ± standard deviation. One-way analysis of variance (ANOVA) or the unpaired Student's t-test were applied to test the significance of the differences between the groups using GraphPad Prism 6.0 (GraphPad Software Inc., San Diego, CA, USA) software. A $p < 0.05$ was considered a significant difference.

## 3. Results and discussion

To break the vicious cycle of ischemia-muscle atrophy-ischemia in ASO-induced lower extremity ischemia, our present work aimed to realize neovascularization and skeletal muscle restoration through our ADSC/FGF19@μsphere system. This system was designed to achieve vasculogenesis and myogenesis simultaneously while exerting the synergistic therapeutic effect of FGF19 and ADSCs, which would have a grand clinical application in ASO-induced lower extremity ischemia.

### 3.1. Microfluidic GelMA microspheres serve as FGF19 and ADSCs carriers

In order to construct the FGF19-loaded stem cell carriers, we chose GelMA as our starting material, as GelMA has previously exhibited significant cell adhesive properties and drug loading capability previously. The degree of methacrylation of GelMA was determined by NMR. Based on the NMR analysis, the GelMA exhibited a high degree of methacrylation, 61% (Supplementary Fig. 1). In the first step, FGF19-loaded microfluidic GelMA microspheres were fabricated by adopting our previous protocol with necessary modifications [37]. We added 50 μg FGF19 into the GelMA solution before entering the microfluidic device to ensure that it was incorporated into the microspheres. The GelMA microdroplets with a uniform size of about 180 μm were successfully obtained under pre-determined fabrication parameters (concentration, velocity, etc.) (Fig. 2B). The size of the lyophilized microspheres was 177 μm. After immersed in PBS for 24 h, the microspheres showed a slightly larger size of 179 μm due to a small amount of swelling. The particle sizes were normally distributed and showed good dispersibility (Fig. 2J and K). To evaluate the microsphere stiffness, the mechanical

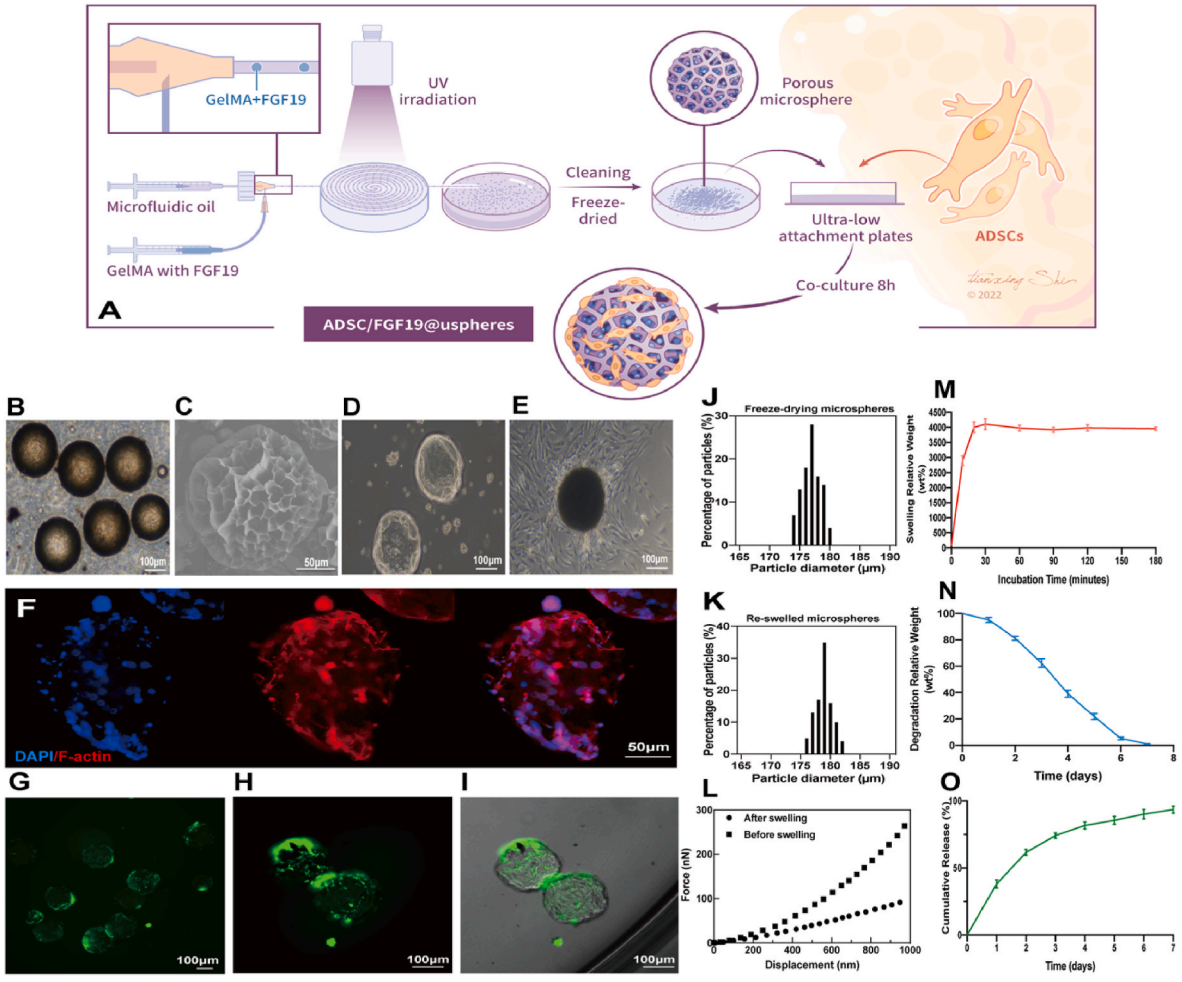


**Fig. 2. Characterization of FGF19-loaded GelMA microsphere.** A) Schematic diagram of microfluidic technology to fabricate porous microspheres and loading of ADSCs. B) Gross view of FGF19-loaded GelMA microspheres. C) SEM images of the freeze-drying FGF19-loaded GelMA microspheres from the overall view. D) Image of FGF19-loaded GelMA microsphere cultured with ADSCs for 1 h in low attachment plate. E) Gross view of ADSCs growth after adhesion to FGF19-loaded GelMA microspheres. F) Fluorescence microscopic confocal image of microspheres loaded with ADSCs stained by rhodamine phalloidin. G) Live/Dead assay of ADSCs loading on FGF19-loaded GelMA microspheres at low magnification. Live cells (green) are labelled with calcein AM and dead cells (red) are labelled with ethidium homodimer. H&I) Live/Dead assay of ADSCs loading on FGF19-loaded GelMA microspheres at high magnification and brightfield view. J) Particle size distribution of freeze-drying microspheres. K) Particle size distribution of re-swelled microspheres. L) Microsphere force-displacement curve measured using nanoindentation assisted by atomic force microscopy. M) The swelling ratio of FGF19-loaded GelMA microspheres. N) The degradation profile of FGF19-loaded GelMA microspheres. O) Release curves of FGF19 releasing from GelMA microspheres.

behavior was measured by the atomic force microscopy with a nano-indentation technique (Fig. 2L). According to their force-displacement behavior curves, their elastic modulus was calculated using Hertz contact mechanics theory. The elastic moduli of freeze-drying and re-swelled microspheres were 25.6 kPa and 14.7 kPa, respectively. Moreover, these microspheres demonstrated a highly porous structure with pore sizes between 20 and 40 μm after freeze-drying, which provided an enormous surface area for stem cell loading and adhesion (Fig. 2C). The GelMA FGF19-microspheres rapidly absorbed a large amount of liquid as the weight of microspheres increased by 41-fold after 30 min soaking in aqueous solution (Fig. 2M). The stability of FGF19-loaded microspheres was then assessed by monitoring their degradation behavior in aqueous solution. According to the degradation analysis, the mass loss of FGF19-microspheres increased with time, with complete degradation obtained by day 7 in 2 U $mL^{-1}$ collagenase solution (Fig. 2N), which suggests that FGF19-microspheres could respond well to the biological environment. According to the results of the morphology of the degradation process using SEM, it could be observed that the microspheres could maintain their basic structure in the early stage (within 3 days), and the degradation rate was accelerated with the gradual reduction of the mass (Supplementary Fig. 2). In the follow-up release experiment, a classical two-stage release curve of FGF19 was observed: a relatively fast release phase in the first 3 days, followed by a more sustained second phase. After 7 days, FGF19 achieved a release rate of over 95% (Fig. 2O). It has been reported that FGF19 can improve muscle loss and achieve muscle protection at an early stage [29,30]. Therefore, the fast release curve of the FGF19-loaded in this microsphere system may be beneficial to muscle tissue recovery.

Such large liquid absorbance capability, combined with the porous structure formed during freeze-drying makes the microspheres excellent carriers for stem cell delivery as the stem cells can be easily absorbed onto the microspheres from their suspension [32]. The ADSCs and FGF19-loaded GelMA microspheres were co-cultured in low-attachment plates so that the microsphere surface served as the only adsorbable surface for cells (Fig. 2D). Cells in low-attachment plates maintained a spherical unattached appearance, but the ADSCs expanded into polygonal shapes after attachment to the microsphere surface. Then, the ADSC-loaded microspheres were transferred onto normal culture plate to allow ADSC to migrate. ADSCs on the microspheres were observed to climb out of the microspheres and proliferate approximately to the microspheres. The migrated cells exhibited similar morphology to standard cultured ADSCs, suggesting the ADSCs maintained their status on the microspheres (Fig. 2E). This indicates that the FGF19-loaded GelMA microspheres did not affect the growth and migration ability of cells.

Using the internal porous structure of GelMA microspheres, drugs and bioactive factors can be loaded by physical doping, and the purpose of minimally invasive delivery and the controlled release of drugs can be achieved at the lesion site [25]. The microspheres have efficient cell adhesion ability, which is conducive to the carrying of stem cells and improves the efficiency of therapy [32]. At the same time, microspheres scaffolds containing cytokines and stem cells can improve the level of the repair system. In this study, the engineered microspheres were delivered to the site of the lesion by intramuscular injection, which reduced the trauma caused by treatment and promoted the efficiency.

### 3.2. ADSCs maintained excellent proliferative and migration capability in GelMA microspheres

It was observed that almost all ADSCs automatically attached onto the microspheres after overnight culture on the ultralow attachment plates. In the evaluation system of stem cell delivery, cell survival, proliferation and migration capability are 3 important indicators popularly used in the biomaterials community. Firstly, we showed that ADSCs distributed homogenously on the surface of the microspheres and exhibited well-organized F-actins (Fig. 2F), indicating that GelMA microspheres provided ADSCs a good surface to adhere. Then, we used live-dead staining to characterize the survival of ADSCs on microspheres. Large amounts of living cells were clearly observed on the surface of the microspheres. No dead cells were detected on the microspheres as dead cells tend to detach from microsphere surface once they lose their integrity (Fig. 2G–I). Cell survival on the microspheres could be maintained for at least 21 days (Supplementary Fig. 3), demonstrating cyto-compatibility of the microspheres. Next, ADSCs were cultured on the conventional plates and GelMA microspheres, respectively in order to compare cell proliferation rate on different substrates with the CCK-8 assay. The results showed that ADSCs grown on GelMA microspheres had similar proliferative activity in the first 3 days compared to those grown on culture plates. With the extension of the incubation time (5 and 7 days), the cell viability kept on increasing on microspheres (Fig. 3A). Due to the large specific surface area of the microsphere compared to 2-dimensional (2D) plates [25,38,39], it is rational to speculate that when implanted *in vivo*, GelMA microspheres as ADSC carriers may provide sufficient surface area for cell expansion and survival.

We next used the transwell assay and the scratch wound healing assay to investigate ADSCs migration ability after grown on microspheres. We observed that both the number of migrated cells and the closure of the wound showed no statistical significance between the two groups, respectively. The ADSCs grown on GelMA microspheres had similar migration ability to those grown on culture plates (Fig. 3B–E), indicating that ADSCs maintained their functional activity on the microspheres. The normal migration capability of ADSCs on GelMA microspheres provided the foundation for regulating homeostasis and mediating tissue repair.

Taken together, these results demonstrated that the GelMA microsphere was a promising ADSCs carrier, as it exhibited the following advantages: i) ADSCs could be loaded conveniently without complicated operations; ii) GelMA microspheres showed high cell loading capacity, enabling abundant ADSCs density at the lesion; and iii) ADSCs could maintain functionality and proliferatively activity on the GelMA microspheres.

### 3.3. ADSCs exhibited great angiogenesis capability on GelMA microspheres

We found that ADSCs on GelMA microspheres exhibited good biocompatibility and high cell-loading capacity. We subsequently investigated the relationship between ADSCs loading density on GelMA microspheres and the angiogenic potential of ADSCs, and whether FGF19-loading microspheres could promote the angiogenic potential of ADSCs comparing to blank microspheres, as ADSCs largely exert their therapeutic effects via angiogenic enhancement derived from paracrine secretion.

Firstly, the expression of major extracellular matrix (ECM) components was analyzed after allowing ADSCs to grow on GelMA microspheres and FGF19-loading microspheres at different seeding densities for an extended culture time. As shown in Fig. 3F, the gene expression of key ECM components proportionally increased when the cell density on the blank microspheres increased. The same trend could also be observed in FGF19-loading microspheres, but the expression levels were higher. This observation was further confirmed via Western blot. In the blank microspheres, semi-quantification of protein expression showed that fibronectin, laminin, and collagen I and IV expression in the high-density group increased by 3.8, 3.7, 2.6, and 4.2 folds, respectively, compared to the low-density counterpart (Fig. 3H). Moreover, compared with blank microspheres, these protein expressions were further increased by 15%, 16%, 11%, and 28%, respectively, when the high densities of ADSCs were loaded into the FGF19-loading microspheres, suggesting that the FGF19-loading microspheres allowed high-density cell survival, which led to higher production of ECM proteins. Similarly, the secretion of angiogenic factors (*e.g.*, HGF, bFGF, and VEGF) was also proportional with the density of ADSCs seeded on the

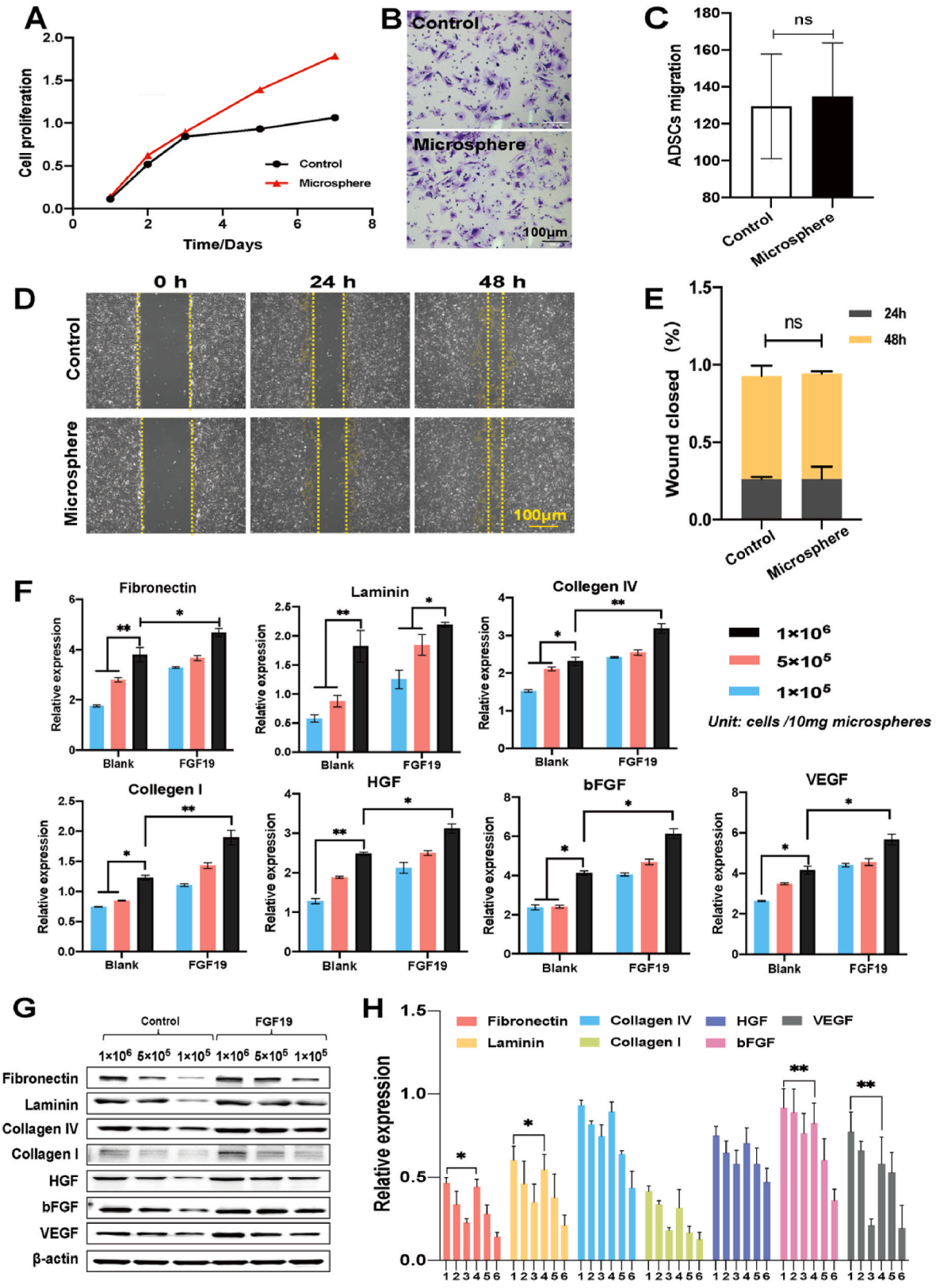


**Fig. 3. Proliferation, migration and angiogenesis performance of ADSCs on GelMA microspheres.** A) The proliferation curves of ADSCs seeded on culture plate and GelMA microspheres. B) ADSCs grown on indicated substrates were subjected to a transwell migration assay and C) the results of statistical evaluation results. D) ADSCs grown on indicated substrates were used for an *in vitro* scratching wound healing assay, and E) the results of statistical evaluation results. F) qRT-PCR assay was used to evaluate the gene expression of extracellular matrix (fibronectin, laminin, collagen I and collagen IV) and angiogenic factors (HGF, bFGF and VEGF). Western blot and qRT-PCR outcomes are shown relative to β-actin. (units: cells/10 mg microspheres) G) Western blotting was used to assess fibronectin, laminin, collagen I, collagen IV, HGF, bFGF and VEGF protein expression in the 6 different groups (Group1-3: FGF19-loading microspheres with high, medium and low densities of ADSCs; Group 4–6: Blank microspheres with high, medium and low densities of ADSCs). H) Western blotting data of the levels of fibronectin, laminin, collagen I, collagen IV, HGF, bFGF and VEGF in different groups. Experiments were repeated 3 times. $^{*}p < 0.05$, $^{**}p < 0.01$ and $^{***}p < 0.001$.

microspheres, and the ADSCs on FGF19-loading microspheres could secret more angiogenic factors than that on blank microspheres (Supplementary Fig. 4).

The premise that ADSCs exert a therapeutic effect resets on their ability to successfully survive and graft locally after being delivered [24]. To achieve this, the presence of ECMs is required to establish strong cell-cell and cell-ECM interactions, shielding cells from mechanical insult during injection and forming a functional stem cell niche [40,41]. We expect the microsphere-assisted ADSCs delivery system developed here provided a platform that equipped the ADSCs *in vitro* for better therapeutic effects thanks to the abundant accumulation of ECMs (*e.g.,* fibronectin, laminin, and, collagen I and IV) (Fig. 3F–H), which effectively increased ADSCs retention and engraftment. Moreover, the paracrine secretions of angiogenic factors, such as HGF, bFGF and VEGF, also increased correspondingly (Fig. 3F–H), which validated the significant angiogenesis capability of the ADSCs on the microspheres, and FGF19-loading microspheres further promoted the angiogenesis capability of ADSCs. In short, ADSCs exerted their angiogenesis capability on the FGF19-loading microspheres, and the FGF19-loading microspheres loaded with a high density of ADSCs showed high cell viability, as they not only produced abundant ECMs to provide structural support for their retention and survival but also secreted angiogenic factors to promote neovascularization. Therefore, the delivery of ADSCs via the FGF19-loading microspheres as a carrier holds great promise for applications to lower extremity ischemia re-vascularization.

### 3.4. FGF19-loaded GelMA microsphere promoted functionality of myoblasts in vitro

Given that FGF19 possesses a strong myogenic effect, we then explored how the microsphere behaved as a carrier to achieve the sustained release of FGF19 and maintained its bioactivity *in vitro*. To verify the pro-myogenic effect of FGF19 released from the microspheres, C2C12 cells (myoblasts) were co-cultured with plain GelMA microspheres and FGF19-loaded GelMA microspheres.

Both MyoD and Myf5 are two important regulators in myogenic differentiation; Pax7 is an inducer in skeletal muscle development and remodeling. qRT-PCR was performed to evaluate the expression levels of MyoD, Myf5 and Pax7 (Fig. 4A). After 3 days of culture, the genes (MyoD and Pax7) expression of C2C12 cells on the FGF19-loaded microspheres were significantly higher than those on the plain microspheres. In addition, the expression of MyoD, Myf5 and Pax7 on day 5 were further upregulated and significantly higher in the FGF19-loaded microsphere group. Correspondingly, the Western blot results also showed that the expression of MyoD, Myf5 and Pax7 in the FGF19-loaded microsphere group increased by 364%, 223% and 158% respectively compared to plain microsphere group on day 5 (Fig. 4B and C). In short, the sustained release of FGF19 from the microspheres substantially promoted myogenic markers expression to regulate myogenesis. In addition, the C2C12 migration assay via transwell inserts showed that the migrated C2C12 cells were significantly higher in the FGF19 group. On day 5, the number of migrated C2C12 cells in the FGF19 group were 40% higher than the control group (Fig. 4D and E), indicating that the FGF19-loaded GelMA microspheres displayed a great myoblast recruitment capacity.

It has been reported that S6K1, a downstream target of mTOR, regulates muscle cell growth. ERK1/2 is a well-established target of FGF19 and its downstream targets are also known to regulate mTOR [29,30]. We next detected the phosphorylation levels of S6K1 and ERK1/2 in two groups of C2C12 cells by Western blot (Fig. 4F). In the FGF19-loaded microsphere group, we observed a higher level of phosphorylated S6K1 and ERK1/2, which again validated that the FGF19-loaded microspheres could effectively promote myoblast growth. Taken together, these results suggested that FGF19-loaded GelMA microspheres were able to facilitate myoblasts migration, differentiation and cell growth *in*

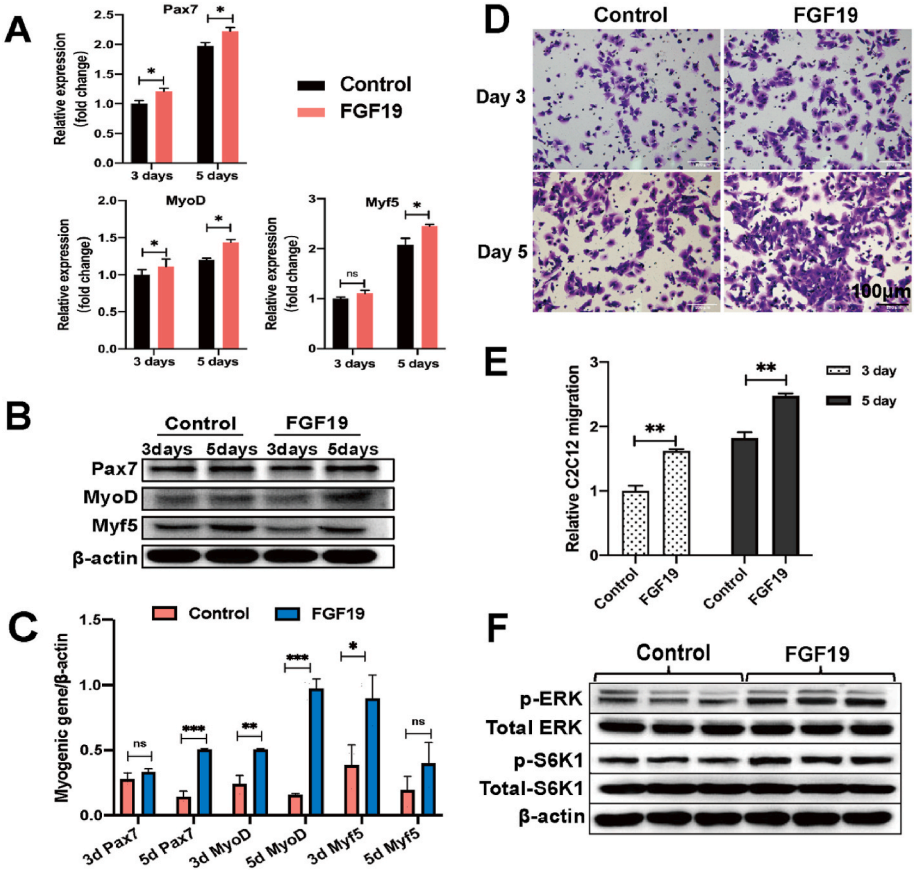


**Fig. 4. The effect of FGF19@μspheres on the migration and myogenesis of C2C12.** A) qRT-PCR assay was used to evaluate the C2C12 cells gene expression of myogenic factors (Pax7, MyoD and Myf5) after treatment with or without FGF19 for 3 and 5 days, with β-actin serving as a normalization control. B) Western blotting was used to assess Pax7, MyoD, and Myf5 protein expression after treatment with or without FGF19 for 3 and 5 days. C) Western blotting data of the levels of Pax7, MyoD, and Myf5 in different groups. Data are shown relative to β-actin. D) C2C12 cells in the indicated treatment groups were subjected to a transwell migration assay, and E) the statistical evaluation results. F) A representative Western blot (3 biological replicates run per gel) of the ERK, p-ERK, S6K1 and p-S6K1 from C2C12 cells treated or not treated by FGF19. The graph indicates the signaling proteins stimulated by FGF19. $^{*}p < 0.05$, $^{**}p < 0.01$ and $^{***}p < 0.001$.

*vitro*, underscoring its potential to enhance myogenesis *in vivo*.

### 3.5. ADSC/FGF19@μspheres exhibited synergy effects in angiogenesis and myogenesis

After confirming that GelMA microspheres could be successfully used for efficient ADSCs delivery, as well as for bioactive FGF19 loading and sustained release, we next sought to investigate whether the combination of ADSCs and FGF19 (ADSCs + FGF19) with the GelMA microsphere could realize myogenesis and angiogenesis simultaneously. More importantly, we intended to assess whether such doubling of effects would achieve a synergy which could augment the regenerative outcomes of limb ischemia.

To investigate whether the co-delivery of FGF19 and ADSCs on the microspheres produced a stronger myogenic effect than the single treatment, we cultured C2C12 cells with microspheres loaded with different variants in a transwell migration assay and a transwell co-culture assay to mimic the ADSC-FGF19-myoblast interaction *in vivo* (Fig. 5A). The migrated C2C12 cells recruited by the different treatment groups in the transwell migration assay were presented in Fig. 5B. Although only a few migrated cells appeared on the membrane in the blank control and the plain microsphere groups, C2C12 cells in the ADSCs + FGF19 group covered large areas of the membrane and displayed strong viability and healthy morphology. Quantification of migrated C2C12 cells suggested that significant enhancement of recruitment efficacy was demonstrated in the ADSCs + FGF19 group, as the migrated cells were 15% and 31% higher than the ADSCs group and FGF19 group, respectively (Fig. 5C). Next, we detected the expression of MyoD in C2C12 cells harvested from different groups in transwell co-culture assay. After co-cultured with various microsphere groups for 3 days, the ADSCs + FGF19 group showed the highest myogenic activity, as the expression of MyoD was significantly upregulated and increased by over 200% compared to the other cell/protein-loaded groups (Fig. 5D and E), supporting that ADSCs and FGF19 acted synergistically in myogenesis *in vitro*.

As we have mainly focused on the influence of the ADSC-FGF19-microsphere system on the myogenic differentiation of C2C12 cells, we have not addressed the question of whether the presence of FGF19 in the system would affect the lineage determination of ADSC down the roads, as we speculated that the enhanced expression of angiogenic and myogenic-related factors of ADSCs in the system may be one of the mechanisms for the synergy effect. Our preliminary experiments found that ADSCs treated with FGF19 underwent enhanced differentiation of both vasculogenic and myogenic lineages (Supplementary Fig. 5).

Hence, we monitored the differentiation-related factors expression of ADSCs seeded on plain microspheres and FGF19-loaded microspheres by CD31 and MyhC immunofluorescence staining. The green fluorescent signal of CD31 was clearly detected in the ADSC/FGF19@μsphere group, while weak fluorescence signals were observed in the ADSCs loaded GelMA microsphere group (Fig. 5F). Quantitative analysis showed that the ADSC-FGF19-microsphere microenvironment significantly increased the expression of CD31 in ADSCs (10 folds higher than the plain microsphere group) (Fig. 5H), suggesting ADSCs acquired an enhanced vasculogenic differential and neovascularization potential. Similarly, the MyhC, a myogenic differential regulator, signal was more obvious in ADSC/FGF19@μsphere group compared to the weak fluorescence signals in the ADSCs loaded GelMA microsphere group (Fig. 5G). The expression of MyhC in the ADSC/FGF19@μsphere group increased by 6 folds compared to the ADSCs loaded GelMA microsphere group (Fig. 5H), which revealed that the ADSC-FGF19-microsphere microenvironment also enhanced the myogenic differential potential of the ADSCs. We speculate that the synergistic effect of myogenesis observed in the above experiment may be related to it, and ADSCs may promote the myogenesis of C2C12 cells via paracrine secretion under the effect of FGF19. In short, we found that ADSC/FGF19@μsphere not only enabled the ADSCs and FGF19 to act synergistically on myoblasts differentiation, but also enhanced the differentiation potential of ADSCs in both vasculogenic and myogenic directions.

### 3.6. ADSC/FGF19@μspheres substantially improved blood perfusion and muscle strength of hindlimb ischemia in vivo

To validate the feasibility of using ADSC/FGF19@μspheres for hindlimb ischemia treatment *in vivo*, we ligated and clipped the left femoral artery to establish a mouse hindlimb ischemia model. The ischemic sites were injected with plain microspheres, FGF19@μspheres, ADSC @μspheres and ADSC/FGF19@μspheres, respectively (Fig. 6A). The blood perfusion levels of the ischemic limbs were monitored using a dynamic non-invasive Laser Doppler blood flow meter at various time points within the 3-week post-surgical period. On day 0, no significant blood flow signal was detected in all groups, indicating the successful establishment of the ischemic model. A similar observation was obtained on day 3. However, a more obvious blood signals appeared in the ADSC-containing groups while the control and FGF19 groups remained at low signal levels. On day 21, the FGF19 and control groups had the least degree of blood perfusion recovery. The perfusion ratio of the control group only reached 60%, which was due to the host's endogenous repair mechanism. Blood perfusion in blood perfusion in the ADSC/FGF19@μspheres group was more continuous and almost recovered to the level before the ligation (perfusion ratio >90%) (Fig. 6B).

To determine if the ADSCs/FGF19@μspheres could improve the muscle functions, the grip strength and the muscle contraction force of the ischemic hindlimbs were measured by a grip-test meter system within the 3-week period and *ex vivo* after tetanic stimulation, respectively. On day 0, a grip strength of less than 20gf was detected in all mice. Accompanied by the prolonged restoration time, the grip strength in the ADSC-containing groups increased and reached 30gf on day 21, while the FGF19 and control groups remained at less than 25gf (Fig. 7A). The hindlimbs treated with ADSCs/FGF19@μspheres showed 3.9, 3.0, and 1.2-fold increases in muscle mass-normalized contraction force as compared to control, FGF19, and ADSCs treatments (Fig. 7B).

In summary, our data suggested ADSC/FGF19@μsphere system effectively ameliorated tissue ischemia and promoted skeletal muscle functions, as it effectively promoted neovascularization, generated blood reperfusion, and improved the grip strength and contraction force of the ischemia hindlimb *in vivo*.

### 3.7. Histological evaluation of animal experiment

To evaluate the tissue inflammation after implantation, the mice that received saline and different microspheres treatments were sacrificed on day 3. We performed H&E staining to observe the histologic changes and ELISA to detect the levels of inflammatory factors. Except for a slight increase in IL-6 in mice treated with FGF19@μsphere, no severe inflammatory response was observed after microspheres transplantation (Supplementary Fig. 6). To evaluate the regenerative therapeutic performance of the ADSC/FGF19@μsphere system *in vivo*, mice that received different microspheres treatments were sacrificed at day 21, and the skeletal muscles of the ischemic hind limbs were harvested. Firstly, we performed H&E staining to observe the myofibrils restoration after treatment (Fig. 8A). The H&E staining results showed the extensive necrotic and atrophic myofibers (red squares) in the ischemic regions in the control and FGF19 groups. On the contrary, treatment with the ADSC@μspheres and ADSC/FGF19@μspheres achieved successful maintenance of the large muscle fibrils. Notably, more myoblasts (black arrows) were observed in the ADSC/FGF19@μspheres group, suggesting that the ADSC/FGF19@μspheres substantially mobilized the myogenic activity and maintained muscle function after ischemia. Masson's trichrome staining (Fig. 8A) showed a large area of fibrosis in the control and FGF19 groups (black squares). In contrast, the ischemic limbs treated with ADSC@μspheres and ADSC/FGF19@μspheres displayed

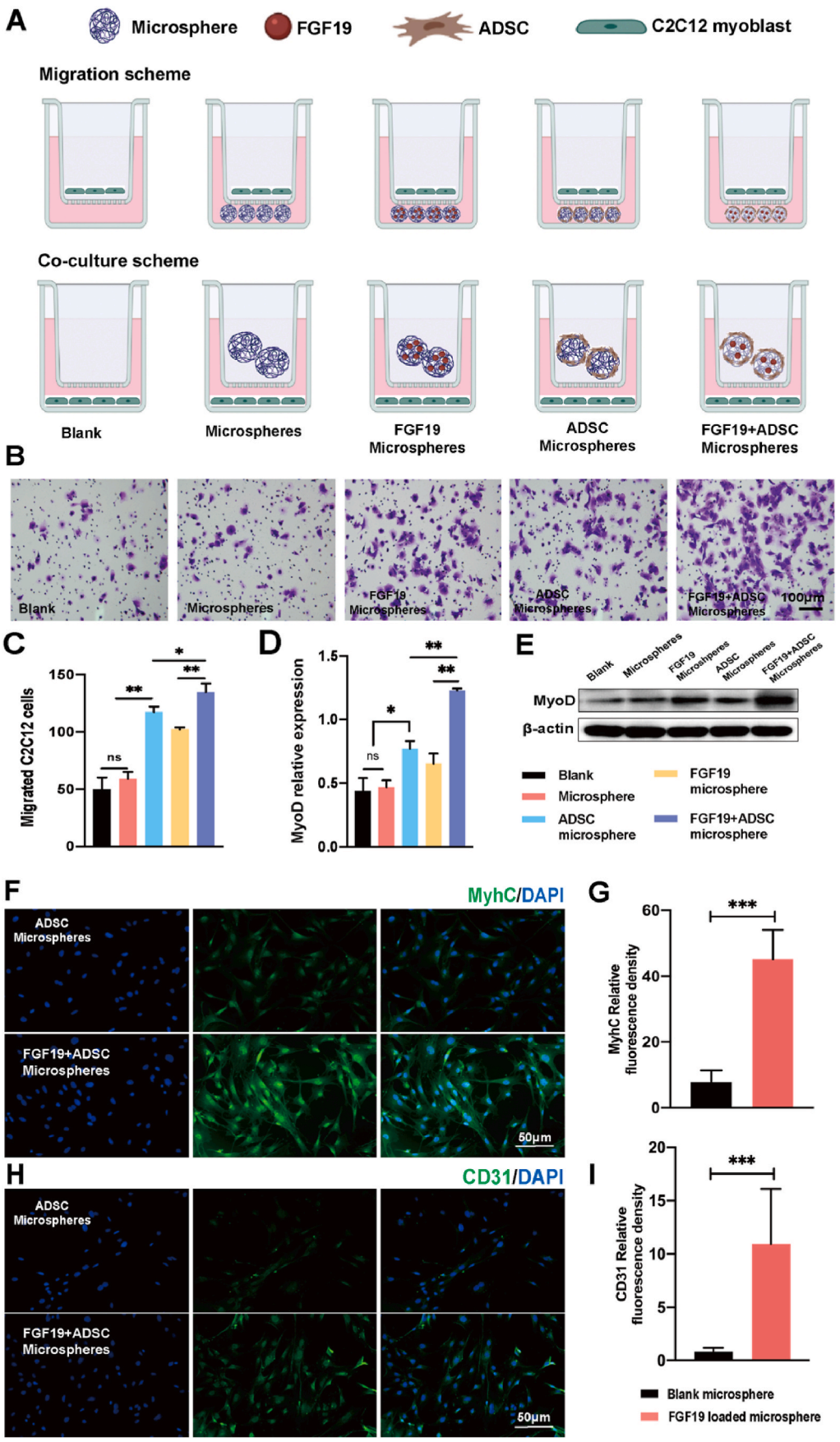


**Fig. 5. A synergy myogenic performance of ADSC/FGF19@μsphere *in vitro*.** A) Schematic illustration of investigation of the synergy effect of ADSCs and FGF19. In migration scheme, C2C12 cells were seeded in the 8 μm upper chambers and different microspheres were put in the lower chambers. In co-culture scheme, the different microspheres were put in the 0.4 μm upper chambers and C2C12 were seeded in the lower chambers. B) The migrated C2C12 cells in the migration scheme of different groups, and C) the results are presented as the number of the migrated cells. D&E) In co-culture scheme, western blotting was used to assess MyoD protein expression of the C2C12 cells in different groups, and the data are shown relative to β-actin. F) Laser scanning confocal microscopy images of fluorescently labelled MyhC (green) in ADSCs seeded on the blank microspheres and FGF19@μspheres, and G) the results of relevant statistical analysis. H) Laser scanning confocal microscopy images of fluorescently labelled CD31 (green) in ADSCs seeded on the blank microspheres and FGF19@μspheres, and I) the results of relevant statistical analysis. $^{*}p < 0.05$, $^{**}p < 0.01$ and $^{***}p < 0.001$.

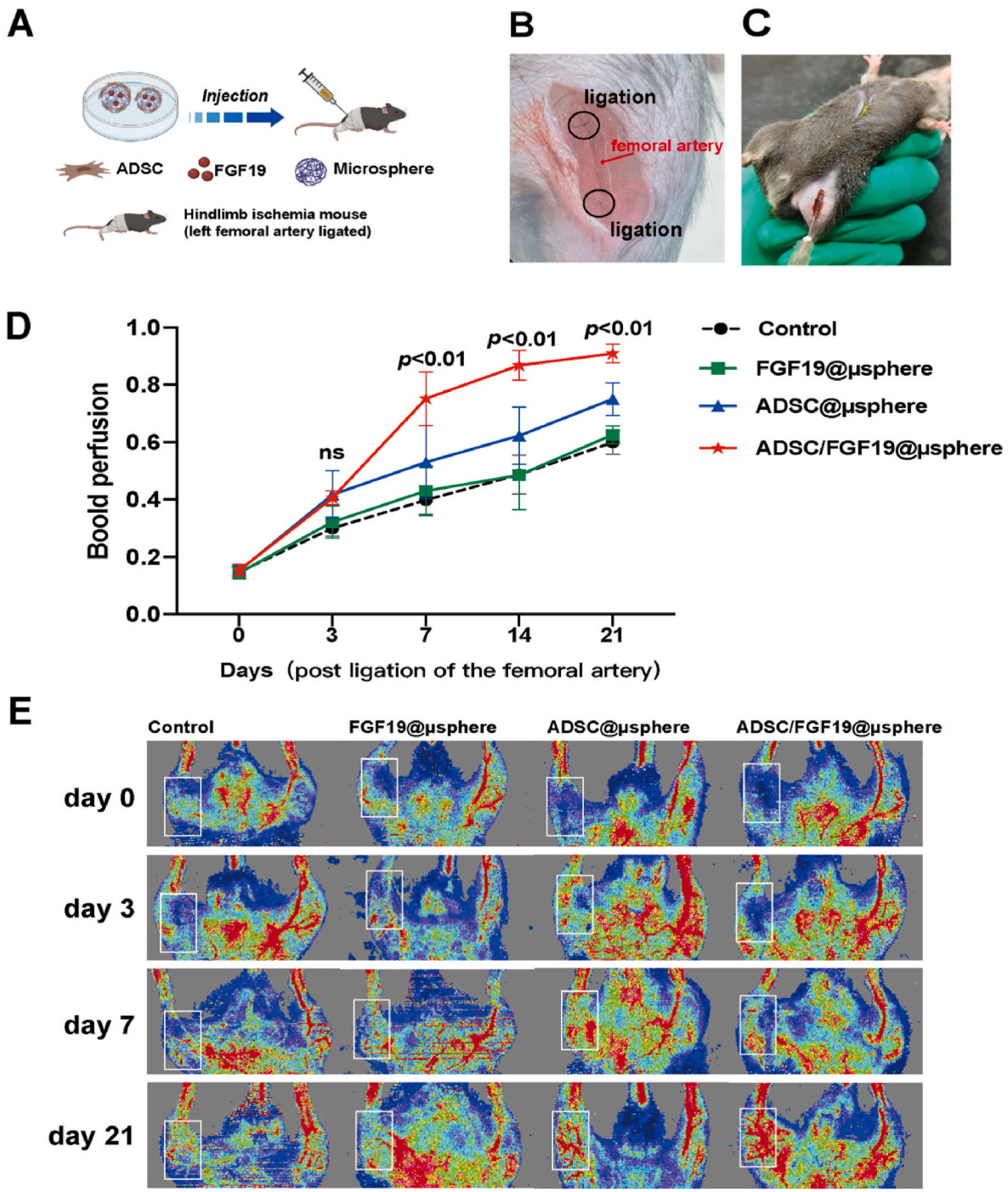


**Fig. 6. Dynamic evaluation of blood perfusion recovery *in vivo*.** A) Schematic of the ADSC/FGF19@μspheres treatment. B) Representative photographs of limb ischemia modeling. C) Injection of microspheres into the ischemic region. D) Blood perfusion ratio curves of the ischemic regions after different treatments. Blood perfusion ratios were normalized to the average blood perfusion in the ROI region of the normal hindlimb. E) Representative laser Doppler images obtained after ADSC/FGF19@μspheres and other indicated treatments injection treatments on days 0, 3, 7, and 21, respectively. The white squares indicate the blood perfusion changes in the ischemic lesions.

minimal fibrosis. Quantitative analysis showed that the fibrotic area in the control group was 1.6-, 4.3- and 14.4-fold larger than the FGF19, ADSCs and ADSC + FGF19 groups, respectively (Fig. 8B), indicating the ADSC/FGF19@μspheres reduced tissue fibrosis, which substantially prevented irreversible scarring and even loss of muscle function in the ischemic limb.

In order to further verify the *in vivo* activation of the myogenic molecules during the skeletal muscle restoration process after the ADSC/FGF19@μspheres implantation, immunofluorescence staining on MyoD was conducted in the ischemic regions of the 4 groups (Fig. 8A, C). The positive expression of MyoD in the 4 groups was indicated by the red fluorescence signals. It could be observed that MyoD was weakly expressed in the sham group as a control. The expression of MyoD in the other 3 groups was much higher than that in the control group. The ADSC + FGF19 group presented with the strongest expression of MyoD in terms of both areas and density. According to the quantitative analysis of the integrated optical density, the expression of MyoD in the ADSC + FGF19 group was 4.9-fold of that in the control group. After ADSC +

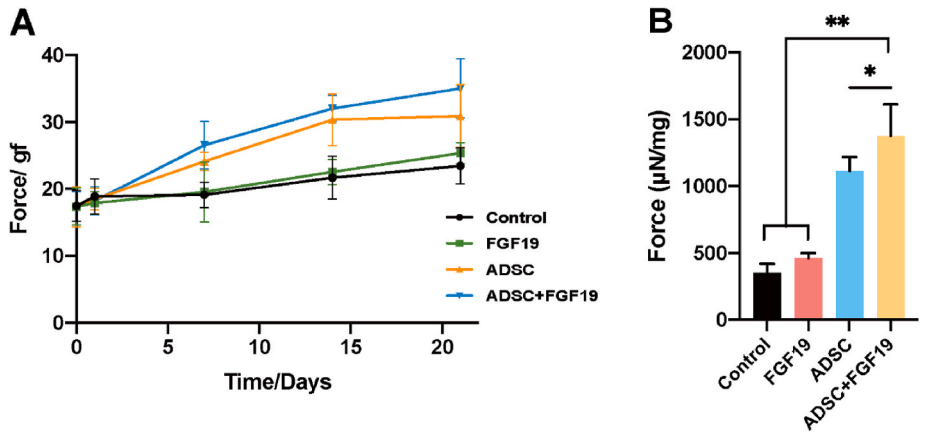


**Fig. 7. Characterization of skeletal muscle function.** A) Grip strength curves of the ischemic hindlimbs after different treatments. B) Maximum muscle contraction force after *ex vivo* stimulation. The contraction forces were normalized to skeletal muscle mass. (n = 6).

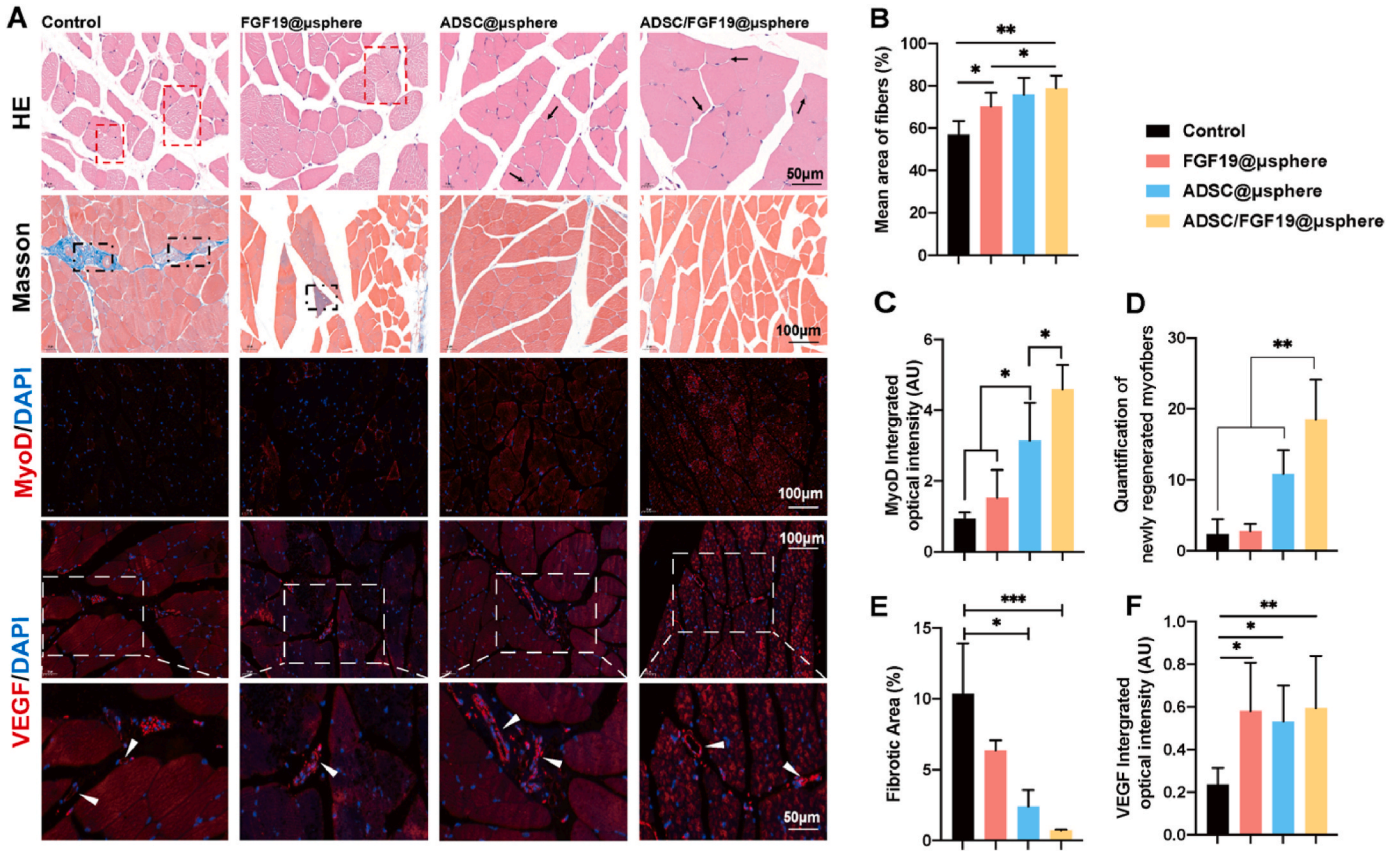


**Fig. 8. *In vivo* treatment of ADSC/FGF19@μspheres generates skeletal muscle restoration and angiogenesis after ischemia (Day 21).** A) H&E staining: Images of H&E staining indicate the myogenic performance of different treatment groups. The red squares highlight the atrophic and damaged myofibrils. The black arrows indicate the presence of myoblasts. Masson's trichrome staining: images of Masson's trichrome staining indicate the anti-fibrosis performance of the different treatment groups. The black squares represent the collagen deposition. MyoD staining: images of MyoD staining indicate the myogenic activity after different treatments. VEGF staining: images of VEGF staining indicate the angiogenic activity after different treatments. The white arrows highlight the new vessels. B) Percentage of the skeletal muscles cross section associated with muscle fibers. C) Quantitative analyses of mean fluorescence intensities of MyoD in different treatment groups. D) Quantitative analyses of newly regenerated myofibers. E) Quantitative analyses of fibrotic area in Masson's trichrome staining. F) Quantitative analyses of mean fluorescence intensities of VEGF in different treatment groups. $^{*}p < 0.05$, $^{**}p < 0.01$, and $^{***}p < 0.001$. (Control: n = 4; FGF19, ADSC, ADSC + FGF19: n = 6).

FGF19 treatment, the number of newly regenerated myofibers was 7.9, 6.6, and 1.7-fold higher than that of control, FGF19, and ADSC groups, respectively. These data further validated the robust skeletal muscle restoring effect of this system, and the synergy effect of myogenesis was also observed *in vivo*. Furthermore, in order to verify the *in vivo* angiogenesis performance in the ischemic tissues of the ADSC/FGF19@μsphere system, we used immunofluorescence staining on VEGF in the ischemic regions of the four groups (Fig. 8A). Red fluorescence signal density indicated the expression level of VEGF. We found that the ADSC + FGF19 group, compared to the control, FGF19 and

ADSC groups, the *in vivo* expression of VEGF was more significant. While the VEGF fluorescence signal was rarely detected in the control group, the ADSC + FGF19 group showed the strongest fluorescence signal. According to the quantitative analysis, the expression of VEGF in the ADSC + FGF19 group increased by 152%, 7%, and 12% compared to the control, FGF19 and ADSC groups, respectively (Fig. 8D), which confirmed that ADSC/FGF19@μsphere system exhibited significant angiogenesis properties in the ischemic regions.

Collectively, our *in vivo* data validated that the ADSC/FGF19@μsphere system simultaneously promoted angiogenesis and myogenesis, and it outperformed the single treatments. Compared with ADSCs or FGF19 alone, we found that the ADSC/FGF19@μsphere treatment accelerated the re-perfusion in the ischemic region (Fig. 6B). Besides, it minimized the fibrotic and atrophic areas, as the fibrotic areas of *ADSCs + FGF19: ADSCs: FGF19 = 1:3.3:9* (Fig. 8B), which reduced permanent damage to skeletal muscle structure and function. Moreover, tissues with great myogenic performance showed consistent elevations in angiogenic performance (MyoD: +4.9-fold and VEGF: +1.5-fold Fig. 8D), which demonstrated the therapeutic benefit was superior compared to that of ADSCs and FGF19 alone. The above results supported ADSC/FGF19@μsphere system broke the vicious circle of ischemia-muscle atrophy-ischemia, and substantially doubled the regenerative effect of limb ischemia. Inspired by this, we speculated this strategy could further be applied to different fields and clinics, whereby functional cells and cytokines could be delivered and act synergistically to regulate local homeostasis and mediate treatment *in situ*.

## 4. Conclusion

In summary, we designed a cytokine-incorporated stem cell delivery system to restore both blood flow and muscle damage in ischemic limbs. The system was based on sustained FGF19 release *in situ*, combined with the highly efficient delivery of ADSCs via microfluidic assisted microsphere fabrication technique. Our data demonstrated that the sustained delivery of pro-myogenic FGF19 at the lesion substantially promoted myoblasts recruitment, myogenic differentiation and myofibril growth. Meanwhile, the enhancement of the efficiency of ADSCs delivery made ADSCs produce more ECMs and angiogenic factors, which endowed this system with significant angiogenic properties. More importantly, FGF19 and ADSCs acted synergistically in this system. Herein, rapid presence of blood re-perfusion, minimal fibrosis, and a high level of skeletal muscle restoration in the ischemic regions were achieved after the treatment of ADSC/FGF19@μspheres. In conclusion, an effective synergistic capability of myogenesis and angiogenesis *in vivo* was realized after ADSC/FGF19@μsphere treatment, which enabled further development of biomaterial-assisted *in situ* regenerative therapy.

## Author contributions

Ruihan Wang: Conceptualization, Methodology, Investigation and Writing – Original Draft. Fangqian Wang: Conceptualization, Methodology and Writing – Original Draft. Shan Lu: Methodology, Investigation and Software. Bin Gao, Tong Yuan, Chen Yuan and Yuanqing Kan: Investigation and Resources. Daqiao Guo and Yisheng Xu: Formal analysis. Weiguo Fu: Supervision, Writing - Review & Editing. Xiaohua Yu: Supervision, Writing - Review & Editing. Yi Si: Supervision and Resources.

## Submission declaration

The work described has not been published previously and it is not under consideration for publication elsewhere.

## Declaration of competing interest

The authors declare that they have no known competing financial interests or personal relationships that could have appeared to influence the work reported in this paper.

## Acknowledgements

This work was financially supported by the National Natural Science Foundation of China (grant number 8207021027), Shanghai Clinical Research Center for Interventional Medicine (grant number 19MC1910300) and Shanghai Science and Technology Commission (grant numbers 19441906600, 21S31904800).

## Appendix A. Supplementary data

Supplementary data to this article can be found online at https://doi.org/10.1016/j.bioactmat.2023.04.006.

## References

[1] Z. Cai, L. Guo, L. Qi, S. Cui, Z. Tong, J. Guo, Z. Wang, Y. Gu, Midterm outcome of directional atherectomy combined with drug-coated balloon angioplasty versus drug-coated balloon angioplasty alone for femoropopliteal arteriosclerosis obliterans, Ann. Vasc. Surg. 64 (2020) 181–187, https://doi.org/10.1016/j.avsg.2019.06.014.

[2] D. Akagi, K. Hoshina, A. Akai, K. Yamamoto, Outcomes in patients with critical limb ischemia due to arteriosclerosis obliterans who did not undergo arterial reconstruction, Int. Heart J. 59 (2018) 1041–1046, https://doi.org/10.1536/ihj.17-592.

[3] Y. Watanabe, T. Miyata, K. Shigematsu, K. Tanemoto, Y. Nakaoka, M. Harigai, Current trends in epidemiology and clinical features of thromboangiitis obliterans in Japan - a nationwide survey using the medical support system database, Circ. J. 84 (2020) 1786–1796, https://doi.org/10.1253/circj.CJ-19-1165.

[4] A. Farber, R.T. Eberhardt, The current state of critical limb ischemia: a systematic Review, JAMA Surg 151 (2016) 1070–1077, https://doi.org/10.1001/jamasurg.2016.2018.

[5] D. Jocius, D. Vajauskas, A. Skrebunas, M. Gutauskas, A.E. Tamosiunas, Ischemic Muscle Necrosis of Lower Extremities in Peripheral Arterial Disease: the Impact of 99mTc-MDP Scintigraphy on Patient Management, Kaunas), Medicina, 2019, p. 55, https://doi.org/10.3390/medicina55120763.

[6] S. Partovi, A.-C. Schulte, M. Aschwanden, D. Staub, D. Benz, S. Imfeld, B. Jacobi, P. Broz, K.A. Jäger, M. Takes, R.W. Huegli, D. Bilecen, U.A. Walker, Impaired skeletal muscle microcirculation in systemic sclerosis, Arthritis Res. Ther. 14 (2012) R209, https://doi.org/10.1186/ar4047.

[7] J.M. McClung, T.J. McCord, K. Southerland, C.A. Schmidt, M.E. Padgett, T.E. Ryan, C.D. Kontos, Subacute limb ischemia induces skeletal muscle injury in genetically susceptible mice independent of vascular density, J. Vasc. Surg. 64 (2016), https://doi.org/10.1016/j.jvs.2015.06.139, 1101-1111.e2.

[8] K.F. Ma, B. Berends, I.R. Vedder, S. Levolger, M. Gupta, R.C. Schuurmann, J.P.P. M. de Vries, R.P. Bokkers, Quantification of muscle mass in the legs of patients with peripheral arterial occlusive disease: associations between volumetric and cross-sectional single-slice measurements for identification of atrophy and focal sarcopenia, J. Cardiovasc. Surg. 60 (2019) 672–678, https://doi.org/10.23736/S0021-9509.19.11107-X.

[9] A. Adeyemo, C. Johnson, A. Stiene, K. LaSance, Z. Qi, L. Lemen, J.E.J. Schultz, Limb functional recovery is impaired in fibroblast growth factor-2 (FGF2) deficient mice despite chronic ischaemia-induced vascular growth, Growth Factors 38 (2020) 75–93, https://doi.org/10.1080/08977194.2020.1767612.

[10] P. Mathiyalagan, Y. Liang, D. Kim, S. Misener, T. Thorne, C.E. Kamide, E. Klyachko, D.W. Losordo, R.J. Hajjar, S. Sahoo, Angiogenic mechanisms of human CD34(+) stem cell exosomes in the repair of ischemic hindlimb, Circ. Res. 120 (2017) 1466–1476, https://doi.org/10.1161/CIRCRESAHA.116.310557.

[11] H. Jin, C. Quesada, M. Aliabouzar, O.D. Kripfgans, R.T. Franceschi, J. Liu, A. J. Putnam, M.L. Fabiilli, Release of basic fibroblast growth factor from acoustically-responsive scaffolds promotes therapeutic angiogenesis in the hind limb ischemia model, J. Control. Release Off. J. Control. Release Soc. 338 (2021) 773–783, https://doi.org/10.1016/j.jconrel.2021.09.013.

[12] R. Lakshmanan, G. Ukani, M.T. Rishi, N. Maulik, Trimodal rescue of hind limb ischemia with growth factors, cells, and nanocarriers: fundamentals to clinical trials, Can. J. Physiol. Pharmacol. 95 (2017) 1125–1140, https://doi.org/10.1139/cjpp-2016-0713.

[13] R. Kolvenbach, C. Kreissig, E. Ludwig, C. Cagiannos, Stem cell use in critical limb ischemia, J. Cardiovasc. Surg. 48 (2007) 39–44.

[14] A. Liew, T. O'Brien, Therapeutic potential for mesenchymal stem cell transplantation in critical limb ischemia, Stem Cell Res. Ther. 3 (2012) 28, https://doi.org/10.1186/scrt119.

[15] A. Adamičková, A. Gažová, M. Adamička, N. Chomaničová, S. Valašková, Z. Červenák, B. Šalingová, J. Kyselovič, Molecular basis of the effect of atorvastatin pretreatment on stem cell therapy in chronic ischemic diseases - critical limb ischemia, Physiol. Res. 70 (2021), https://doi.org/10.33549/physiolres.934718. S527–S533.

[16] H. Tanioka, S. Miyagawa, D. Mori, K.-I. Watanabe, T. Ueno, K. Toda, T. Shibuya, T. Kuratani, Y. Sawa, New cell delivery system CellSaic with adipose-derived

stromal cells promotes functional angiogenesis in critical limb ischemia model mice, J. Artif. Organs Off. J. Japanese Soc. Artif. Organs. 24 (2021) 343–350, https://doi.org/10.1007/s10047-021-01254-8.
[17] E. Pilny, R. Smolarczyk, M. Jarosz-Biej, A. Hadyk, A. Skorupa, M. Ciszek, Ł. Krakowczyk, N. Kułach, D. Gillner, M. Sokół, S. Szala, T. Cichoń, Human ADSC xenograft through IL-6 secretion activates M2 macrophages responsible for the repair of damaged muscle tissue, Stem Cell Res. Ther. 10 (2019) 93, https://doi.org/10.1186/s13287-019-1188-y.
[18] H. Nakagami, K. Maeda, R. Morishita, S. Iguchi, T. Nishikawa, Y. Takami, Y. Kikuchi, Y. Saito, K. Tamai, T. Ogihara, Y. Kaneda, Novel autologous cell therapy in ischemic limb disease through growth factor secretion by cultured adipose tissue-derived stromal cells, Arterioscler. Thromb. Vasc. Biol. 25 (2005) 2542–2547, https://doi.org/10.1161/01.ATV.0000190701.92007.6d.
[19] G. Marino, F. Rosso, P. Ferdinando, A. Grimaldi, G. De Biasio, G. Cafiero, M. Barbarisi, A. Barbarisi, Growth and endothelial differentiation of adipose stem cells on polycaprolactone, J. Biomed. Mater. Res. A. 100 (2012) 543–548, https://doi.org/10.1002/jbm.a.33296.
[20] F. Colazzo, F. Alrashed, P. Saratchandra, I. Carubelli, A.H. Chester, M.H. Yacoub, P. M. Taylor, P. Somers, Shear stress and VEGF enhance endothelial differentiation of human adipose-derived stem cells, Growth Factors 32 (2014) 139–149, https://doi.org/10.3109/08977194.2014.945642.
[21] M. Deng, Y. Gu, Z. Liu, Y. Qi, G.E. Ma, N. Kang, Endothelial differentiation of human adipose-derived stem cells on polyglycolic acid/polylactic acid mesh, 2015, Stem Cell. Int. (2015), 350718, https://doi.org/10.1155/2015/350718.
[22] R. Madonna, S. Delli Pizzi, L. Di Donato, A. Mariotti, L. Di Carlo, E. D'Ugo, M. A. Teberino, A. Merla, A. Tartaro, R. De Caterina, Non-invasive in vivo detection of peripheral limb ischemia improvement in the rat after adipose tissue-derived stromal cell transplantation, Circ. J. 76 (2012) 1517–1525, https://doi.org/10.1253/circj.cj-11-1215.
[23] H.M. Thai, E. Juneman, J. Lancaster, T. Hagerty, R. Do, L. Castellano, R. Kellar, S. Williams, G. Sethi, M. Schmelz, M. Gaballa, S. Goldman, Implantation of a three-dimensional fibroblast matrix improves left ventricular function and blood flow after acute myocardial infarction, Cell Transplant. 18 (2009) 283–295, https://doi.org/10.3727/096368909788535004.
[24] Y. Li, W. Liu, F. Liu, Y. Zeng, S. Zuo, S. Feng, C. Qi, B. Wang, X. Yan, A. Khademhosseini, J. Bai, Y. Du, Primed 3D injectable microniches enabling low-dosage cell therapy for critical limb ischemia, Proc. Natl. Acad. Sci. U. S. A 111 (2014) 13511–13516, https://doi.org/10.1073/pnas.1411295111.
[25] J. Yang, J. Liang, Y. Zhu, M. Hu, L. Deng, W. Cui, X. Xu, Fullerol-hydrogel microfluidic spheres for in situ redox regulation of stem cell fate and refractory bone healing, Bioact. Mater. 6 (2021) 4801–4815, https://doi.org/10.1016/j.bioactmat.2021.05.024.
[26] T. Freyman, G. Polin, H. Osman, J. Crary, M. Lu, L. Cheng, M. Palasis, R. L. Wilensky, A quantitative, randomized study evaluating three methods of mesenchymal stem cell delivery following myocardial infarction, Eur. Heart J. 27 (2006) 1114–1122, https://doi.org/10.1093/eurheartj/ehi818.
[27] L. Zhang, Y. Li, C. Zhang, M. Chopp, A. Gosiewska, K. Hong, Delayed administration of human umbilical tissue-derived cells improved neurological functional recovery in a rodent model of focal ischemia, Stroke 42 (2011) 1437–1444, https://doi.org/10.1161/STROKEAHA.110.593129.
[28] H. Kim, H.Y. Kim, M.R. Choi, S. Hwang, K.-H. Nam, H.-C. Kim, J.S. Han, K.S. Kim, H.S. Yoon, S.H. Kim, Dose-dependent efficacy of ALS-human mesenchymal stem cells transplantation into cisterna magna in SOD1-G93A ALS mice, Neurosci. Lett. 468 (2010) 190–194, https://doi.org/10.1016/j.neulet.2009.10.074.
[29] B. Benoit, E. Meugnier, M. Castelli, S. Chanon, A. Vieille-Marchiset, C. Durand, N. Bendridi, S. Pesenti, P.A. Monternier, A.C. Durieux, D. Freyssenet, J. Rieusset, E. Lefai, H. Vidal, J. Ruzzin, Fibroblast growth factor 19 regulates skeletal muscle mass and ameliorates muscle wasting in mice, Nat. Med. 23 (2017) 990–996, https://doi.org/10.1038/nm.4363.
[30] H. Kurosu, M. Choi, Y. Ogawa, A.S. Dickson, R. Goetz, A.V. Eliseenkova, M. Mohammadi, K.P. Rosenblatt, S.A. Kliewer, M. Kuro-O, Tissue-specific expression of βklotho and Fibroblast Growth Factor (FGF) receptor isoforms determines metabolic activity of FGF19 and FGF21, J. Biol. Chem. 282 (2007) 26687–26695, https://doi.org/10.1074/jbc.M704165200.
[31] J. Wang, H. Zhao, L. Zheng, Y. Zhou, L. Wu, Y. Xu, X. Zhang, G. Yan, H. Sheng, R. Xin, L. Jiang, J. Lei, J. Zhang, Y. Chen, J. Peng, Q. Chen, S. Yang, K. Yu, D. Li, Q. Xie, Y. Li, FGF19/SOCE/NFATc2 signaling circuit facilitates the self-renewal of liver cancer stem cells, Theranostics 11 (2021) 5045–5060, https://doi.org/10.7150/thno.56369.
[32] X. Zhao, S. Liu, L. Yildirimer, H. Zhao, R. Ding, H. Wang, W. Cui, D. Weitz, Injectable stem cell-laden photocrosslinkable microspheres fabricated using microfluidics for rapid generation of osteogenic tissue constructs, Adv. Funct. Mater. 26 (2016) 2809–2819, https://doi.org/10.1002/adfm.201504943.
[33] A. Limbourg, T. Korff, L.C. Napp, W. Schaper, H. Drexler, F.P. Limbourg, Evaluation of postnatal arteriogenesis and angiogenesis in a mouse model of hind-limb ischemia, Nat. Protoc. 4 (2009) 1737–1748, https://doi.org/10.1038/nprot.2009.185.
[34] T.M. Raimondo, D.J. Mooney, Functional muscle recovery with nanoparticle-directed M2 macrophage polarization in mice, Proc. Natl. Acad. Sci. U. S. A 115 (2018) 10648–10653, https://doi.org/10.1073/pnas.1806908115.
[35] C.A. Cezar, E.T. Roche, H.H. Vandenburgh, G.N. Duda, C.J. Walsh, D.J. Mooney, Biologic-free mechanically induced muscle regeneration, Proc. Natl. Acad. Sci. U. S. A 113 (2016) 1534–1539, https://doi.org/10.1073/pnas.1517517113.
[36] T.M. Raimondo, D.J. Mooney, Anti-inflammatory nanoparticles significantly improve muscle function in a murine model of advanced muscular dystrophy, Sci. Adv. 7 (2021) 1–11, https://doi.org/10.1126/sciadv.abh3693.
[37] J. Wu, G. Li, T. Ye, G. Lu, R. Li, L. Deng, L. Wang, M. Cai, W. Cui, Stem cell-laden injectable hydrogel microspheres for cancellous bone regeneration, Chem. Eng. J. 393 (2020), https://doi.org/10.1016/j.cej.2020.124715.
[38] Y. Xu, Y. Gu, F. Cai, K. Xi, T. Xin, J. Tang, L. Wu, Z. Wang, F. Wang, L. Deng, C. L. Pereira, B. Sarmento, W. Cui, L. Chen, Metabolism balance regulation via antagonist-functionalized injectable microsphere for nucleus pulposus regeneration, Adv. Funct. Mater. 30 (2020) 1–14, https://doi.org/10.1002/adfm.202006333.
[39] Y. Sun, Q. Zhou, Y. Du, J. Sun, W. Bi, W. Liu, R. Li, X. Wu, F. Yang, L. Song, N. Li, W. Cui, Y. Yu, Dual biosignal-functional injectable microspheres for remodeling osteogenic microenvironment, Small (2022), 2201656, https://doi.org/10.1002/smll.202201656, 2201656.
[40] E.S. Novoseletskaya, O.A. Grigorieva, A.Y. Efimenko, N.I. Kalinina, Extracellular matrix in the regulation of stem cell differentiation, Biochemistry. (Mosc). 84 (2019) 232–240, https://doi.org/10.1134/S0006297919030052.
[41] F. Gattazzo, A. Urciuolo, P. Bonaldo, Extracellular matrix: a dynamic microenvironment for stem cell niche, Biochim. Biophys. Acta 1840 (2014) 2506–2519, https://doi.org/10.1016/j.bbagen.2014.01.010.